Received December 17, 2020, accepted December 26, 2020, date of publication December 30, 2020, date of current version January 12, 2021.

Digital Object Identifier 10.1109/ACCESS.2020.3048184

Joint Compressed Sensing and Spread Spectrum Through-the-Wall Radar Imaging

MINCHAO LI[1], XIAOLI XI[1], (Member, IEEE), XUEHUI ZHANG[2], AND GAOHUI LIU[1]

[1]Institute of Advanced Navigation and Electromagnetics, Xi'an University of Technology, Xi'an 710048, China

[2]Beijing Huahang Radio Measurement Institute, Beijing 100013, China

Corresponding author: Xiaoli Xi (xixiaoli@xaut.edu.cn)

This work was supported in part by the National Natural Science Foundation of China under Grant 61671375.

ABSTRACT High-resolution radar imaging has to be accomplished within the constraints of aperture size, frequency, and acquisition time. To achieve effective and reliable imaging, we introduce a compressed sensing (CS) technology to spread spectrum through-the-wall radar imaging. Using the sparseness of the spread spectrum through-the-wall radar echo in the correlation domain and the sparsity of the target information in the imaging region, the feasibility of CS technology for reducing the number of observation points and the number of samples per observation point is verified. Moreover, considering the high sensitivity of CS technology to clutter, receiver cancellation is adopted to remove the strong clutter information present in echo signals. The results of numerical simulations show that CS technology can provide very efficient sampling, thereby significantly reducing the amount of data required. Compared to back-projection imaging based on traditional sampling technology, the proposed CS technique can obtain almost the same satisfactory resolution and quality imaging results using only 0.72% of the total data. This will reduce the hardware costs and significantly shorten the data-acquisition and data-transfer times.

INDEX TERMS Compressed sensing, radar imaging, signal processing, spread spectrum, through-the-wall.

I. INTRODUCTION

Counterterrorism, disaster relief, fire assistance, and building layout determination require the detecting of objects behind obstacles. Compared with other penetration technologies, through-the-wall radar imaging (TWRI) has gained research interest owing to its good penetrability and high-resolution imaging capabilities [1], [2]. According to the different signals that are transmitted, through-the-wall radars (TWRs) can be approximately classified into impulse radar, stepped-frequency continuous wave radar, frequency modulated continuous wave radar, noise radar, and pseudorandom noise radar [3]. As a type of pseudorandom noise radar, spread spectrum radar has been widely applied in TWR surveillance, owing to its easy implementation, low probability of interception, strong anti-noise performance, compact equipment, and accurate time-of-arrival (TOA) estimation [4]–[6].

Considering a spread spectrum TWRI scenario, to obtain sufficiently accurate target imaging results with high resolution in both azimuth and range, large-aperture radar systems and ultra-wideband signals for TWRs are required. However, large-aperture radar systems require costly physical sensors with a large physical aperture, or the placement of single sensors at many different positions to form a large synthetic aperture. This increases the hardware costs, acquisition time, and data storage requirements [7], [8]. Similarly, the wider the bandwidth of the transmitted signal, the higher the sampling frequency of the analog-to-digital converter (ADC) required by the radar receiver; thus, the sampling data will include a large amount of echo data. This places tremendous pressure on the processing, transmission, and storage of the signal. Furthermore, these echo data are mainly redundant, and it is wasteful to acquire and process data samples that will be discarded later. Therefore, new methods for efficient data acquisition are needed to reduce hardware costs and speed up radar imaging.

Compressed sensing (CS) is a signal-processing method used to reconstruct a signal using fewer measurements or signal samples without compromising the imaging quality [9]. CS is an appropriate approach to solve the above-mentioned problems. If the signal is sparse or has a sparse representation in a known dictionary, CS can recover the signal from a small amount of measurement data using a nonlinear algorithm [7].

The associate editor coordinating the review of this manuscript and approving it for publication was Wei Wang.

Because the target behind the wall occupies fewer pixels in the imaging domain, its imaging information is sparse in the spatial domain. Based on this sparsity, Yoon and Amin were the first to use CS technology in stepped-frequency radar imaging [10]. Baraniuk and Steeghs subsequently applied CS to synthetic aperture radar imaging systems that use pulsed chirp or pseudo-noise sequence [11]. Huang *et al.* [12] reported that the amount of data required to reconstruct the target spatial image combined with CS theory is only 7.7% of the delay-and-sum beamforming. Moreover, CS technology was further developed in [13], [14], and [15]. Zhang *et al.* used the singular value decomposition algorithm to obtain the singular value of compressed radar data, and discussed through-the-wall human detection using ultra-wideband radars [13]. Lagunas *et al.* used a reduced set of spatial-frequency observations in stepped-frequency radar platforms to achieve joint wall clutter mitigation and CS application [14]. In [15], CS significantly reduced the number of receivers and could still obtain accurate focus imaging of a target that is behind single or multilayer walls. Zhang *et al.* studied CS with spread spectrum radar, based on the sparsity of target information in the imaging area [16]. When the scene is sparse, CS provides very efficient sampling, which significantly reduces the amount of data required. Therefore, the study of spread spectrum TWRI based on CS technology will help expand the practical uses and application areas of spread spectrum radar.

In this work, considering the spread spectrum TWRI, the transmitted signal was a sine wave modulated by a pseudorandom code (M-sequence), after which its TOA was obtained from the correlation domain after despreading and correlation processing [6], [17]. To reduce the influence of strong clutter on the CS performance, the receiver cancellation method was introduced. Based on the sparseness of the spread spectrum radar echo after demodulation and correlation processing [6], the Gaussian random measurement matrix compresses the time domain signal, and the orthogonal matching pursuit (OMP) algorithm is used to recover the correlation domain data samples from a small number of measured values [18], [19]. Based on the spatial sparseness of the target information in the imaging area, data obtained from fewer observation points are used to complete high-quality imaging of the target behind the wall, which further reduces the total amount of data required for imaging. In this work, we introduced the theoretical basis of this method, and simulated and analyzed the feasibility and performance of CS technology applied to spread spectrum TWRI from many aspects. Numerical simulation results fully prove its effectiveness, and this research promotes the process of practical application of CS technology.

The remainder of this paper is organized as follows: Section II describes the basic theory of CS technology; Section III illustrates how CS is used in the data-acquisition process of spread spectrum radar; Section IV presents the results of numerical simulations and their analysis; concluding remarks are presented in Section V.

II. CS THEORY

This section introduces the basic theory of CS. Further details can be found in [20], [21]. The sparseness or compressibility of signals is an important prerequisite and the theoretical basis for CS technology [22]. Assuming, the original signal $\mathbf{X} \in \mathbf{R}^{N\times 1}$ is S-sparse, $\mathbf{\Phi}$ is a known measurement matrix that projects a high-dimensional signal $\mathbf{X}$ into a low-dimensional space, and the sampling result $\mathbf{Y}$ can be expressed as

$$\mathbf{Y} = \mathbf{\Phi X}. \tag{1}$$

Therefore, the CS problem is to solve the underdetermined equation $\mathbf{Y} = \mathbf{\Phi X}$ to obtain the original signal $\mathbf{X}$ based on the known measured value $\mathbf{Y}$ and the measurement matrix $\mathbf{\Phi}$. However, the general natural signal $\mathbf{X}$ itself is not sparse and requires sparse representation on a sparse basis, i.e.,

$$\mathbf{X} = \mathbf{\Psi \Theta}, \tag{2}$$

where $\mathbf{\Theta} \in \mathbf{R}^{N\times 1}$ is the sparse coefficient vector of $\mathbf{X}$ in dictionary $\mathbf{\Psi} \in \mathbf{R}^{N\times N}$. Then, the final equation can be described as

$$\mathbf{Y} = \mathbf{\Phi X} = \mathbf{\Phi \Psi \Theta} = \mathbf{V \Theta}, \tag{3}$$

where $\mathbf{V} = \mathbf{\Phi \Psi}$ is called the sensing matrix.

Under normal circumstances, the number of equations is significantly smaller than the number of unknowns. The equation has no definite solution and cannot reconstruct the signal. However, because the signal is S-sparse, assuming that $\mathbf{\Phi}$ in the above equation satisfies the restricted isometry property (RIP) [23], the S coefficients can be accurately reconstructed from the M measurements to obtain an optimal solution. Then, the underdetermined equations $\mathbf{Y} = \mathbf{V\Theta}$ can be obtained by solving the problem of minimizing the 0-norm, which is expressed as

$$\min \ \|\mathbf{\Theta}\|_{l_0} \quad s.t.\ \mathbf{Y} = \mathbf{V\Theta}, \tag{4}$$

Knowing $\mathbf{Y}$ and $\mathbf{V}$, and solving $\mathbf{\Theta}$, the original signal $\mathbf{X}$ is then obtained using (2) [14].

III. APPLYING CS IN DATA ACQUISITION OF SPREAD SPECTRUM RADAR

In this section, the data measurement and processing of spread spectrum radar are introduced, and the application of CS for data acquisition is explained.

A. DATA PROCESSING OF SPREAD SPECTRUM RADAR SIGNAL

The transmitted signal of the spread spectrum radar can be expressed as

$$S_T(t) = M_s(t)\sin(2\pi f_0 t), \tag{5}$$

where $M_s(t)$ is an M-sequence (a type of pseudorandom code) of period T_M and f_0 is the center frequency. After despreading and correlation processing, the received signal $\mathbf{R}(n)$ can be transformed from the time domain to the correlation domain,

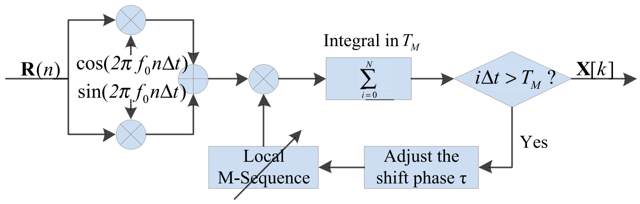

FIGURE 1. Despreading and sliding correlation processing of the spread spectrum radar signal.

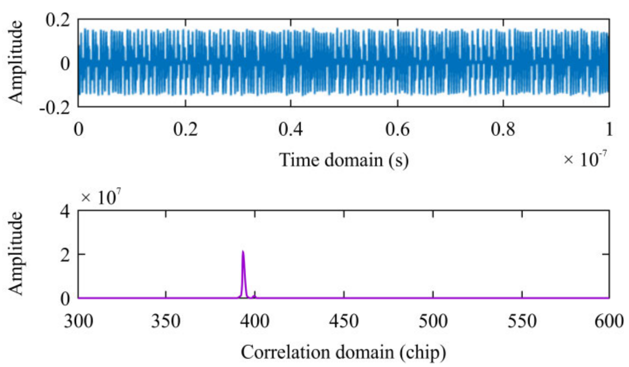

FIGURE 2. Spread spectrum radar time-domain echo signal and its corresponding correlation-domain signal waveform.

and then the TOA of the received signal can be obtained from the peak position in the correlation domain.

The data-processing method [24] adopted in this study is illustrated in Fig. 1. First, $\mathbf{R}(n)$ is multiplied by a sine wave and a cosine wave with center frequency f_0, respectively. Second, after despreading, the signal is multiplied by the locally generated M-sequence, and the integrals for those products are computed over the M-sequence period T_M. Once the time exceeds T_M, the M-sequence is regenerated after a phase shift of $\tau = phase(T_M/(1023))$. The demodulated signal is then multiplied by the regenerated M-sequence. These steps are repeated until 1023 periods of T_M have passed. Finally, the correlation-domain signal $\mathbf{X}[k]$ can be acquired.

Fig. 2 shows a set of time-domain echo signals received by a spread spectrum TWR receiver and its corresponding correlation-domain signal waveform. The time-domain signal does not contain any zero points; thus, it is not sparse. However, after processing the data using the method illustrated in Fig. 1, the signal includes only a few non-zero points, as shown in its corresponding correlation-domain signal waveform. The correlation-domain signal is sufficiently sparse for the application of the CS technique.

B. APPLYING CS IN DATA ACQUISITION

This section explains the application of CS for data acquisition. As shown in Fig. 1, the despreading can be described as

$$\mathbf{R}_{\text{exp}} = \mathbf{R} * e^{-2\pi f_0 t}, \tag{6}$$

where $\mathbf{R}_{\text{exp}}$ is the received signal after despreading. Considering that the M-sequence moves one chip at a time, the correlation processing can be expressed as

$$\begin{bmatrix} M_{s1} & M_{s2} & M_{s3} & \cdots & M_{s1021} & M_{s1022} & M_{s1023} \\ M_{s1023} & M_{s1} & M_{s2} & \cdots & M_{s1020} & M_{s1021} & M_{s1022} \\ M_{s1022} & M_{s1023} & M_{s1} & \cdots & M_{s1019} & M_{s1020} & M_{s1021} \\ M_{s1021} & M_{s1022} & M_{s1023} & \cdots & M_{s1018} & M_{s1019} & M_{s1020} \\ \vdots & \vdots & \vdots & \ddots & \vdots & \vdots & \vdots \\ M_{s4} & M_{s5} & M_{s6} & \cdots & M_{s1} & M_{s2} & M_{s3} \\ M_{s3} & M_{s4} & M_{s5} & \cdots & M_{s1023} & M_{s1} & M_{s2} \\ M_{s2} & M_{s3} & M_{s4} & \cdots & M_{s1022} & M_{s1023} & M_{s1} \end{bmatrix} \times \begin{bmatrix} R_{exp-1} \\ R_{exp-2} \\ R_{exp-3} \\ R_{exp-4} \\ \vdots \\ R_{exp-1021} \\ R_{exp-1022} \\ R_{exp-1023} \end{bmatrix} = \begin{bmatrix} X_1 \\ X_2 \\ X_3 \\ X_4 \\ \vdots \\ X_{1021} \\ X_{1022} \\ X_{1023} \end{bmatrix}$$

$$\mathbf{MJ} * \mathbf{R}_{exp} = \mathbf{X} \tag{7}$$

where M_{si} is the ith chip of the M-sequence (which contains 1023 chips), $\mathbf{MJ}$ is a matrix that includes 1023 shifted M-sequences, $\mathbf{R}_{exp-i}$ is the ith element of the received signal $\mathbf{R}_{exp}$, and X_i is the ith element of the correlation-domain signal $\mathbf{X}$. Equation (7) is an example of the M-sequence including 1023 chips, and can be transformed as

$$\mathbf{R}_{exp} = \mathbf{MJ}^{-1} * \mathbf{X} = \mathbf{\Psi} * \mathbf{X}, \tag{8}$$

where $(\cdot)^{-1}$ is the inverse operation. Similar to Fig. 2, the time-domain signal $\mathbf{R}_{exp}$ contains many non-zero points and the correlation-domain signal $\mathbf{X}$ contains only a few non-zero points; therefore, $\mathbf{R}_{exp}$ is sparse on $\mathbf{MJ}^{-1}$. Thus, $\mathbf{MJ}^{-1}$ can be the dictionary $\mathbf{\Psi}$ of CS. The detailed CS processing procedure is illustrated in Fig. 3.

Before applying CS, the very strong clutter in the received time-domain signal $\mathbf{R}(t)$ must be suppressed, because the CS technique is very sensitive to clutter. After clutter suppression, the signal is demodulated, and $\mathbf{R}_{exp}$ is measured by a known Gaussian random matrix $\mathbf{\Phi}$. The measurement vector $\mathbf{Y}_{J\times 1}$ can then be obtained as

$$\mathbf{Y}_{J\times 1} = \mathbf{\Phi}_{J\times N} * \mathbf{R}_{\text{exp}_{N\times 1}}, \tag{9}$$

where J is the projection measurement dimension. The measurement matrix $\mathbf{\Phi}$ compresses the N-dimensional signal $\mathbf{R}_{\text{exp}}$ into a J-dimensional ($J \ll N$) signal $\mathbf{Y}$. From a physical point of view, the random measurement matrix increases the degree of freedom of the measurement data, thereby reducing the amount of sampled data.

Assuming that $\mathbf{\Phi}$ satisfies the RIP criterion, the CS theory can first solve the sparse coefficient $\mathbf{\Theta}$ by solving the inverse problem of (3). Then, it can correctly recover the signal $\mathbf{X}$ with S-sparse from the M-dimensional measured projection value $\mathbf{Y}$. This is a 0-norm minimization problem (see (4)), which is a nondeterministic polynomial complete problem;

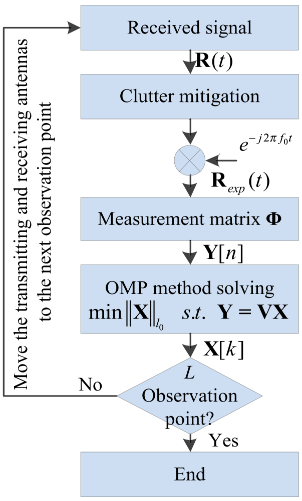

FIGURE 3. Data-processing flow of the application of CS for data acquisition of spread spectrum radar.

thus, it is often transformed into a 1-norm minimization problem:

$$\min \ \|\mathbf{X}\|_{l_1} \quad s.t.\ \mathbf{Y} = \mathbf{V}\mathbf{X}. \tag{10}$$

At present, the OMP is the most important reconstruction algorithm in CS. The computational complexity of the OMP algorithm is $O(J^2S^2)$. It is implemented as follows:

Step 1: Initialize the residual $\mathbf{r}_0 = \mathbf{Y}$, number of iterations $t = 1$. $\mathbf{V}_0$is an empty matrix, index set $\mathbf{\Lambda}_0$ is empty.

Step 2: Select the column number of the column most relevant to the margin $nt = \arg \max_{j=1,\cdots,N} (\mathbf{r_{t-1}}, \mathbf{V}_j)$ in $\mathbf{V}$, and store it in the index set $\mathbf{\Lambda}_t = \mathbf{\Lambda}_{t-1} \cup nt$.

Step 3: Update the selected column space $\mathbf{V}_t = \left[\mathbf{V}_{t-1}, \mathbf{V}_j\right]$.

Step 4: Solve the least-squares problem by QR decomposition, ensuring the minimum residual, and update the vector $\hat{\mathbf{\Theta}} = \arg \min_{\hat{\Theta}} \left\| \mathbf{Y} - \mathbf{V}_t \hat{\mathbf{\Theta}} \right\|_2$.

Step 5: Update the residual $\mathbf{r}_t = \mathbf{Y} - \mathbf{V}_t \hat{\mathbf{\Theta}}$.

Step 6: If the stopping condition $t = S$ is achieved, stop the OMP operation. Otherwise, set $t = t + 1$ and return to Step 2.

IV. NUMERICAL SIMULATIONS AND RESULTS ANALYSIS

This section verifies the feasibility of applying CS in the data acquisition of spread spectrum radar and analyzes the factors that influence the results of TWRI with CS.

A. DETECTION ENVIRONMENT

To reduce the hardware costs and time required for analyzing the factors that influence TWRI [25], we adopted a full-wave simulation technique—specifically, the finite-difference time-domain (FDTD) method [26]—to simulate the signal. The FDTD method is an accurate approach for numerous electromagnetic applications. It is formulated by discretizing Maxwell's curl equations over a finite volume and approximating the derivatives with centered difference approximations. The FDTD method requires a large number of data update calculations, and the running time of the program that computes the simulated signal is significantly lengthened, especially because a complete spread spectrum cycle needs to be simulated. The C# programming language, the TeeChart plug-in (Visual Studio 2012), and the parallel computing capabilities of the CUDA$^{\text{TM}}$ architecture graphics card GPU (NVidia GeForce GTX 760) are used for FDTD programming, which greatly reduces the signal simulation time.

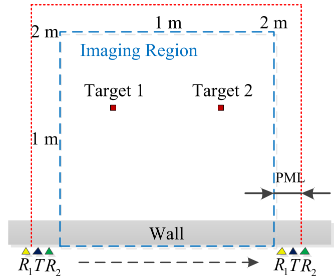

FIGURE 4. FDTD through-the-wall model.

As shown in Fig. 4, a two-dimensional FDTD through-the-wall model was developed with a spatial size of $\Delta x = \Delta y = 0.5$ cm and time-step of$\Delta t = 8.333$ ps. The imaging region was a 2 m $\times$ 2 m rectangle and the thickness of the perfectly matched layer (PML) was 0.5 m. The targets were metal squares with side lengths of 5 cm. There were two targets in the region, with coordinates of (0.5 m, 1.25 m) and (1.5 m, 1.25 m). The thickness, conductivity, and permittivity of the wall were 20 cm, 0.03, and 4.5, respectively. The transmitter $T(-0.5$ m, 0 m) and two receivers ($R_1(-0.55$ m, 0 m) and $R_2(-0.45$ m, 0 m)) were placed next to the wall. The transmitter antenna T transmits a spread spectrum signal with a central frequency of 2 GHz and an M-sequence frequency also of 2 GHz; the spread spectrum signal includes 1023 chips. Once a signal is received at one observation point, the transmitter and receivers move to the next observation point simultaneously. They move simultaneously 151 times at 2 cm intervals.

The time-domain echoes of 151 observation points complete the projection measurement of CS through the same measurement matrix $\mathbf{\Phi}$ (projection measurement dimension $J = 500$); thus, the total amount of data was 500 $\times$ 151. After reconstruction by the OMP method, the relevant domain information of all observation points was obtained and converted into a TOA signal, as shown in Fig. 5(a). The TOA signal recovered by all the observation points was processed by the BP imaging algorithm to complete the target imaging [27], as shown in Fig. 5(b). Only clear wall information is obtained in the image, with no information on the target image behind the wall.

The traditionally sampled TOA signal and its BP imaging results are shown in Figs. 5(c) and 5(d), respectively. In the imaging results, the wall and target information are visible. The ADC parameters are 2 GHz and 16 bits. Comparing Figs. 5(b) and 5(d), there is a significant difference in imaging results, which indicates that CS projection measurements are

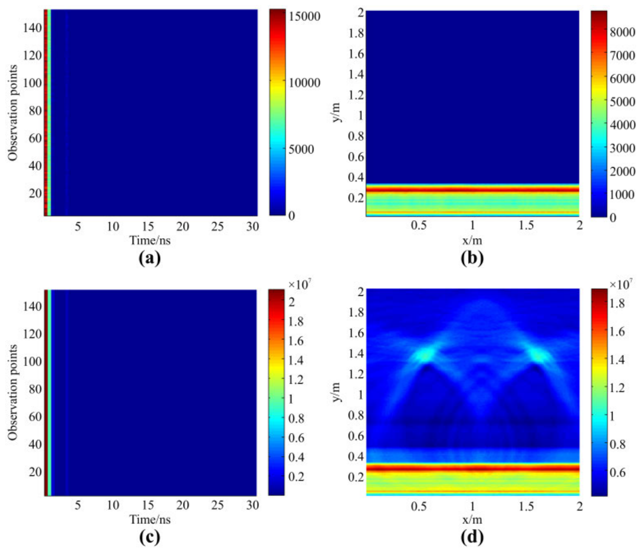

FIGURE 5. Comparison of CS projection measurement and traditional ADC sampling measurement imaging results. (a) TOA signal recovered after CS projection measurement, (b) BP imaging result of (a), (c) traditionally sampled TOA signal, (d) BP imaging result of (c).

very sensitive to direct waves and wall clutter with strong amplitudes. Therefore, before the measurement matrix is used for CS projection measurement, we need to suppress the strong clutter in the echo signal.

B. CLUTTER MITIGATION METHODS

Clutter mitigation is very important for TWRI, because strong direct waves and clutter reflected from the wall will reduce the ability of the OMP algorithm to recover TOA signals. Thus, in this section, we introduce several clutter mitigation methods.

The first clutter mitigation is background subtraction [28], which is the ideal approach because clutter can be removed completely. However, background subtraction needs to measure the same scene both with and without the targets, which is impossible in practical applications. The second method is adaptive exponential averaging [29], which is one of the most widely applied methods for clutter mitigation. However, the receiver cannot guarantee that the two sets of echoes measured at different observation points will have the same start times. The direct wave and wall-reflected wave information in the two sets of echoes cannot be consistent, so adaptive exponential averaging cannot be used for CS clutter elimination processing.

The third method is receiver cancellation, which is illustrated in Fig. 6. The spacing of the receiving antennas (R_1 and R_2) and the transmitting antenna T remains consistent and as small as possible to avoid dispersion of the target information energy after the clutter is removed. The echoes received at R_1 and R_2 are directly cancelled, and the obtained signals are recorded as $\mathbf{R}_d(t)$. Signals $\mathbf{R}_1(t)$ and $\mathbf{R}_d(t)$ are simultaneously projected and measured, and the measurement vectors $\mathbf{Y}_d$ and $\mathbf{Y}$ are obtained and reconstructed by the OMP algorithm. We can then compute the correlation-domain vectors

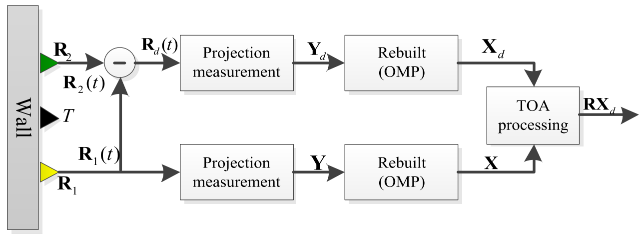

FIGURE 6. Diagram of receiver cancellation processing.

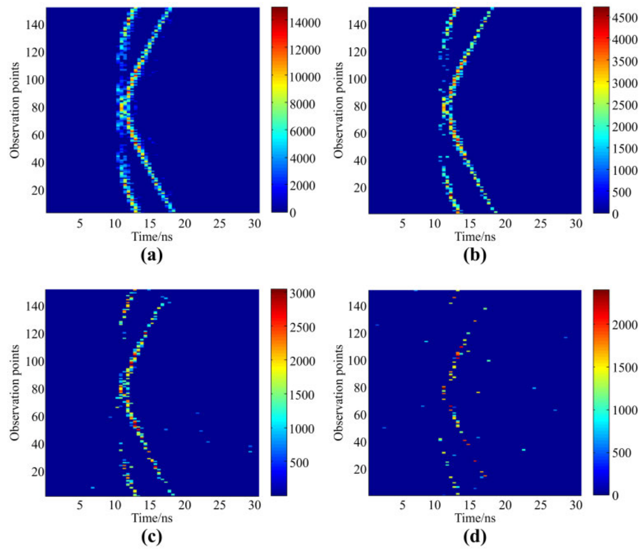

FIGURE 7. Influence of projection measurement dimension on TOA signal recovery. (a) J = 500, (b) J = 50, (c) J = 20, (d) J = 10.

$\mathbf{X}_d$ and $\mathbf{X}$. Signal $\mathbf{X}$ only recovers direct waves and strong clutter, and signal $\mathbf{X}_d$ only recovers the target information. $\mathbf{X}_d$ will then refer to the direct wave position information in signal $\mathbf{X}$ to complete the conversion of the correlation-domain signal to the TOA signal.

C. MEASUREMENT DIMENSION ANALYSIS

The projection measurement dimension J directly affects the number of observations required. In this study, we set J = 500, 50, 20, and 10, respectively, and performed projection measurements and reconstruction on the cancellation echo $\mathbf{R}_d(t)$ of 151 observation points. The restored TOA signal is shown in Fig. 7. As J decreases, the recovery of the target information in the TOA signal declines, especially for the area where the aggregation of the target information is damaged by the receiver cancellation method. Obviously, the larger the value of J, the better the recovered TOA signal. However, the total amount of data required for the CS projection measurement will also be greater. Therefore, it is necessary to find a suitable measurement dimension J based on the recovery requirements.

The TOA signals shown in Fig. 7 were processed by the BP imaging algorithm; the results are presented in Fig. 8. Comparing the four subfigures, it can be seen that the imaging result for $J = 50$ is no worse than that for $J = 500$, and

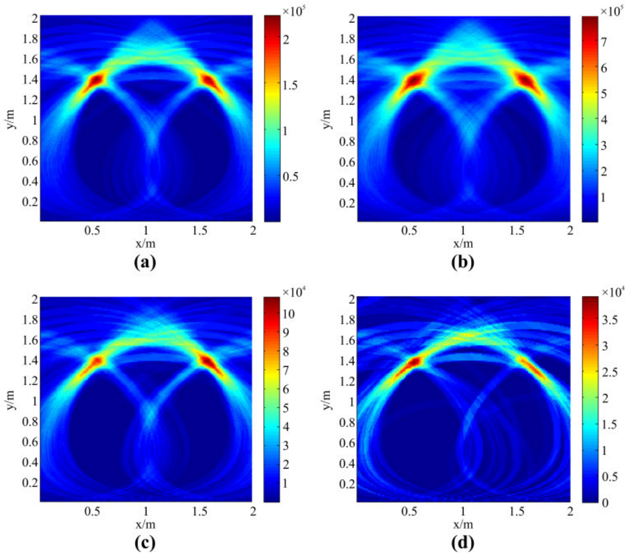

FIGURE 8. Influence of projection measurement dimension on BP imaging results. (a) J = 500, (b) J = 50, (c) J = 20, (d) J = 10.

the erythema in the focal area is actually smaller. This also explains from another perspective that a large J is not always beneficial. The imaging result for $J = 20$ is slightly worse than that for $J = 50$; however, the red spot representing the target can still be clearly identified. When $J = 10$, the red spot becomes slender and unfocused, although both targets can still be identified.

Comparing the amount of data required to generate Figs. 5(d) and 8(c), it is apparent that the CS projection measurement reduces the total amount of data required for imaging, from at least 1023×151 to 20×151. The CS technology significantly reduces the amount of data collected by the spread spectrum TWR and reduces the data storage and operation requirements.

D. ROBUST PERFORMANCE ANALYSIS

TWR functions in complex environments with external noise that are likely to have a significant impact on target detection imaging. In this section, we focus on the robust performance of the CS approach for spread spectrum TWRI. Gaussian white noise with $SNR = 20dB$ was added to the echo signals; the obtained TOA signal is shown in Fig. 9. Comparing Figs. 7(b) and 9(a), it can be seen that when $J = 50$, the presence of noise significantly interferes with the recovery effect of the TOA signal. Most of the target information could not be successfully recovered, and many error messages appeared in the developed algorithm. When $J = 120$, most of the target information in the TOA signal was restored.

Fig. 10 shows the results of BP imaging using the above TOA information. It can be observed that increasing J can significantly improve the imaging quality of the target. When the CS projection measurement technique is used for the spread spectrum TWR, the robust performance can be improved by increasing the projection measurement dimension J. In summary, CS projection measurement

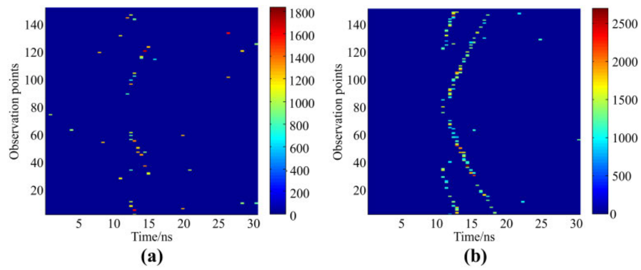

FIGURE 9. Effect of noise on TOA signal recovery. (a) J = 50, SNR = 20 dB, (b) J = 120, SNR = 20 dB.

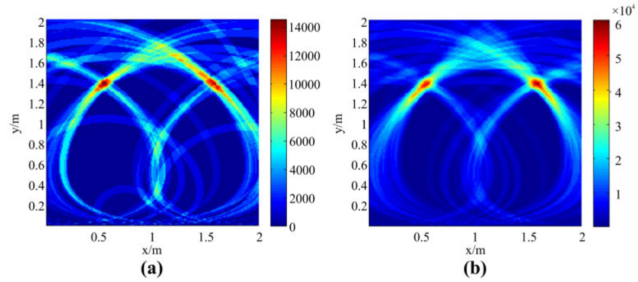

FIGURE 10. Effect of noise on the results of BP imaging. (a) J = 50, SNR = 20 dB, (b) J = 120, SNR = 20 dB.

technology is feasible in practical applications of spread spectrum TWRI.

E. FEASIBILITY OF REDUCING THE NUMBER OF OBSERVATION POINTS

Although the number of measurements per observation point has been reduced from 1023 to 20 by the application of CS technology, BP imaging still uses data from 151 observation locations. To reduce the total amount of data required for imaging further, this section explores the feasibility of using CS technology to reduce the number of observation points.

In general, the number of target pixels in the imaging region is much smaller than the total number of pixels therein. Therefore, in theory, the sparsity of the target information in the imaging region can be utilized to complete the imaging of the target by CS technology. Fig. 11 compares BP imaging and CS imaging results under different amounts of data. The CS technology was executed on an Inter(R) Core(TM) i5-6500 CPU @ 3.2 GHz, with 8 GB DDR4 2133 MHz memory. The runtime of the experiment was 574.4 s.

Figs. 11(a) and 11(b) show the target image obtained by the BP algorithm. The ADC sample length is 1023, and the echo data of four and nineteen observation points are extracted at equal intervals. The total data volume is 1023×4. Fig. 11(c) is a BP imaging result using partial data (35×4). Fig. 11(e) shows the clear target image obtained by the CS algorithm [30] and the total data volume is 35×4. Obviously, the CS algorithm reduces the total amount of data required for spread spectrum TWRI to 0.72% ($(35 \times 4)/(1023 \times 19) = 0.72\%$) of the BP algorithm. Comparing Figs. 11(a), 11(c), and 11(e), the total amount of data used for CS imaging is not only much less than that for BP imaging, but the

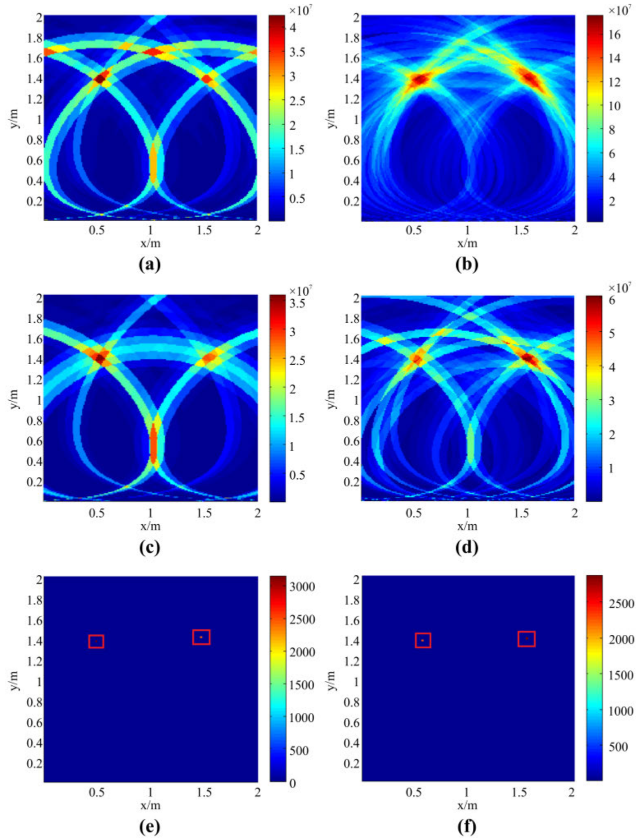

FIGURE 11. Comparison of BP imaging and CS imaging results under different total amounts of data. (a) BP imaging (1023 × 4), (b) BP imaging (1023 × 19), (c) Partial data BP imaging (35 × 4), (d) Partial data BP imaging (20 × 6), (e) CS imaging (35 × 4), (f) CS imaging (20 × 6).

proposed technique also obtains better imaging results, which verifies that CS can be applied to each observation point. The amount of data and the number of observation points have both been reduced, and the data requirements for spread spectrum TWRI have been decreased.

When the CS projection measurement dimension $M = 20$, the total amount of data is 20×4, and the CS imaging result is very poor. This indicates that CS technology cannot reduce the total amount of imaging data without limitation. When the number of observation points increases to six, the total amount of data rises to 20×6 and the CS imaging result is improved, as shown in Fig. 11(f). This indicates that increasing the number of observation points when the CS projection measurement dimension J is low can improve the CS imaging result.

F. TWRI FOR A HUMAN BODY

In TWRI, the most interesting detection target is the human body. The dielectric constant of the human body is tested in the frequency range of 1 GHz to 3 GHz, wherein a uniform dielectric human body model replaces the complete human body model [31], as shown in Fig. 12(a). In Fig. 12(b), an approximate ellipse is used to represent the standard human body cross section (0.35 m × 0.25 m) and the center

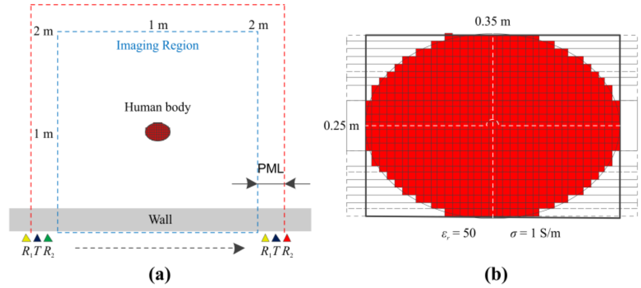

FIGURE 12. Comparison of BP imaging and CS imaging results of a human body. (a) TWRI of a human body, (b) Standard human body cross section (0.35 m × 0.25 m).

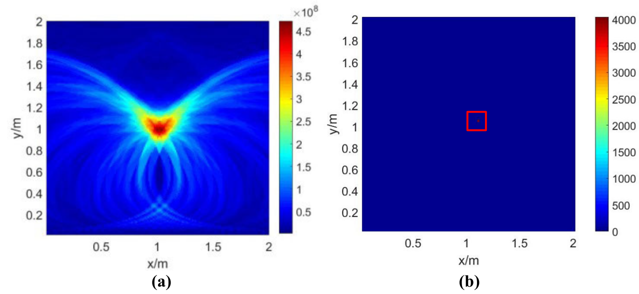

FIGURE 13. Comparison of BP imaging and CS imaging results for a human body. (a) BP human body imaging (1023 × 35), (b) CS human body imaging (35 × 6).

point coordinates (1 m, 1 m); the parameters of the human body model are $\varepsilon_r = 50$ and $\sigma = 1$ S/m.

Using partial data BP imaging (1023×35) and CS imaging (35×6), we obtained the imaging results for a human body as shown in Fig. 13(a) and Fig. 13(b). By comparing these two results, it can be clearly seen that the result of CS imaging is clear and there is less clutter, which further verifies the effectiveness of CS technology.

V. CONCLUSION

In this study, we verified the feasibility of combining CS technology with spread spectrum TWR to reduce the total imaging data requirements. Although the receiver cancellation method may affect the target information, it can remove the strong clutter very effectively, making it possible to combine CS projection measurement with spread spectrum TWR. At each observation point, the amount of data to be measured by spread spectrum TWR can be significantly reduced, alleviating the requirement of data storage during operation. Compared with BP imaging, CS technology can reduce the total amount of data required for imaging, using just 0.72% of the total data used by spread spectrum TWR, and can achieve the same excellent image resolution as fully sampled data without threshold processing. In addition, the CS projection measurement completes the high-frequency "analog sampling" in the analog signal domain, significantly reducing the requirements of the spread spectrum TWR for ADCs and related processing circuits. Moreover, the latest signal recovery algorithm can shorten the calculation time, improve the reconstruction accuracy, and enhance the robustness of the reconstructed signal to noise. Therefore, the combination of CS technology and spread spectrum TWR has extensive application and actual measurements will be conducted in future work.

REFERENCES

[1] P. K. M. Nkwari, S. Sinha, and H. C. Ferreira, "Through-the-Wall radar imaging: A review," *IETE Tech. Rev.*, vol. 35, no. 6, pp. 631–639, Nov. 2018, doi: 10.1080/02564602.2017.1364146.

[2] F. H. C. Tivive, A. Bouzerdoum, and M. G. Amin, "A subspace projection approach for wall clutter mitigation in Through-the-Wall radar imaging," *IEEE Trans. Geosci. Remote Sens.*, vol. 53, no. 4, pp. 2108–2122, Apr. 2015, doi: 10.1109/TGRS.2014.2355211.

[3] F. Fioranelli, "Through-the-wall detection using ultra wide band frequency modulated interrupted continuous wave signals," Ph.D. dissertation, Durham Univ., Durham, U.K., 2013.

[4] R. Zetik, J. Sachs, and R. Thoma, "UWB short-range radar sensing–The architecture of a baseband, pseudo-noise UWB radar sensor," *IEEE Instrum. Meas. Mag.*, vol. 10, no. 2, pp. 39–45, Apr. 2007, doi: 10.1109/MIM.2007.364960.

[5] D. Kocur, M. Švecová, and J. Rováková, "Through-the-Wall localization of a moving target by two independent ultra wideband (UWB) radar systems," *Sensors*, vol. 13, no. 9, pp. 11969–11997, Sep. 2013, doi: 10.3390/s130911969.

[6] X. Zhang, X. Xi, Z. Song, S. Wang, M. Wan, and D. Wu, "Performance analysis of spread spectrum through wall radar," *IEEE Trans. Magn.*, vol. 50, no. 11, Nov. 2014, Art. no. 5102004, doi: 10.1109/TMAG.2014.2330826.

[7] S. Liu, Y. D. Zhang, T. Shan, and R. Tao, "Structure-aware Bayesian compressive sensing for frequency-hopping spectrum estimation with missing observations," *IEEE Trans. Signal Process.*, vol. 66, no. 8, pp. 2153–2166, Apr. 2018, doi: 10.1109/TSP.2018.2806351.

[8] U. Alkus, A. B. Sahin, and H. Altan, "Stand-off through-the-wall W-band millimeter-wave imaging using compressive sensing," *IEEE Geosci. Remote Sens. Lett.*, vol. 15, no. 7, pp. 1025–1029, Jul. 2018, doi: 10.1109/LGRS.2018.2817591.

[9] G. A. Moeness, "Compressive sensing for through-the-wall radar imaging," *J. Electron. Imag.*, vol. 22, no. 3, pp. 030901-1–030901-21, 2013, doi: 10.1117/1.JEI.22.3.030901.

[10] Y.-S. Yoon and M. G. Amin, "Compressed sensing technique for high-resolution radar imaging," in *Proc. Signal Process., Sensor Fusion, Target Recognit.*, Orlando, FL, USA, Apr. 2008, Art. no. 69681A, doi: 10.1117/12.777175.

[11] R. Baraniuk and P. Steeghs, "Compressive radar imaging," in *Proc. IEEE Radar Conf.*, Boston, MA, USA, Apr. 2007, pp. 128–133, doi: 10.1109/RADAR.2007.374203.

[12] Q. Huang, L. Qu, B. Wu, and G. Fang, "UWB through-wall imaging based on compressive sensing," *IEEE Trans. Geosci. Remote Sens.*, vol. 48, no. 3, pp. 1408–1415, Mar. 2010, doi: 10.1109/TGRS.2009.2030321.

[13] B. Zhang and W. Wang, "Through-wall detection of human being with compressed UWB radar data," *EURASIP J. Wireless Commun. Netw.*, vol. 2013, no. 1, Dec. 2013, Art. no. 123, doi: 10.1186/1687-1499-2013-162.

[14] E. Lagunas, M. G. Amin, F. Ahmad, and M. Najar, "Joint wall mitigation and compressive sensing for indoor image reconstruction," *IEEE Trans. Geosci. Remote Sens.*, vol. 51, no. 2, pp. 891–906, Feb. 2013, doi: 10.1109/TGRS.2012.2203824.

[15] W. Zhang and A. Hoorfar, "A generalized approach for SAR and MIMO radar imaging of building interior targets with compressive sensing," *IEEE Antennas Wireless Propag. Lett.*, vol. 14, pp. 1052–1055, 2015, doi: 10.1109/LAWP.2015.2394746.

[16] X. Zhang, X. Xi, Y. Pu, C. Zheng, and D. Wu, "Compressive sensing for through-wall imaging with spread spectrum radar," in *Proc. IEEE MTT-S Int. Wireless Symp. (IWS)*, Shanghai, China, Mar. 2016, pp. 1–4, doi: 10.1109/IEEE-IWS.2016.7585489.

[17] C. Zheng, X. Xi, Z. Song, and K. Zhang, "Multilevel delay lock loop approach for wall clutter mitigation in through-the-wall radar imaging," *IET Microw., Antennas Propag.*, vol. 12, no. 12, pp. 1986–1992, Oct. 2018, doi: 10.1049/iet-map.2018.5234.

[18] T. T. Cai and L. Wang, "Orthogonal matching pursuit for sparse signal recovery with noise," *IEEE Trans. Inf. Theory*, vol. 57, no. 7, pp. 4680–4688, Jul. 2011, doi: 10.1109/TIT.2011.2146090.

[19] M. Yang and F. de Hoog, "Orthogonal matching pursuit with thresholding and its application in compressive sensing," *IEEE Trans. Signal Process.*, vol. 63, no. 20, pp. 5479–5486, Oct. 2015, doi: 10.1109/TSP.2015.2453137.

[20] D. L. Donoho, "Compressed sensing," *IEEE Trans. Inf. Theory*, vol. 52, no. 4, pp. 1289–1306, Apr. 2006.

[21] M. A. Herman and T. Strohmer, "High-resolution radar via compressed sensing," *IEEE Trans. Signal Process.*, vol. 57, no. 6, pp. 2275–2284, Jun. 2009, doi: 10.1109/TSP.2009.2014277.

[22] E. Candès and J. Romberg, "Sparsity and incoherence in compressive sampling," *Inverse Problems*, vol. 23, no. 3, pp. 969–985, Jun. 2007, doi: 10.1088/0266-5611/23/3/008.

[23] E. J. Candès, J. K. Romberg, and T. Tao, "Stable signal recovery from incomplete and inaccurate measurements," *Commun. Pure Appl. Math.*, vol. 59, no. 8, pp. 1207–1223, Aug. 2006, doi: 10.1002/cpa.20124.

[24] S. U. Qaisar and A. Dempster, "Cross-correlation performance assessment of global positioning system (GPS) L1 and L2 civil codes for signal acquisition," *IET Radar Sonar Nav.*, vol. 5, no. 3, pp. 195–203, 2011, doi: 10.1049/iet-rsn.2009.0207.

[25] X. Zhang, X. Xi, M. Li, and D. Wu, "Comparison of impulse radar and spread-spectrum radar in through-wall imaging," *IEEE Trans. Microw. Theory Techn.*, vol. 64, no. 3, pp. 699–706, Mar. 2016, doi: 10.1109/TMTT.2015.2508791.

[26] K. Yee, "Numerical solution of initial boundary value problems involving Maxwell's equations in isotropic media," *IEEE Trans. Antennas Propag.*, vol. 14, no. 3, pp. 302–307, May 1966, doi: 10.1109/TAP.1966.1138693.

[27] L. M. H. Ulander, H. Hellsten, and G. Stenstrom, "Synthetic-aperture radar processing using fast factorized back-projection," *IEEE Trans. Aerosp. Electron. Syst.*, vol. 39, no. 3, pp. 760–776, Jul. 2003, doi: 10.1109/TAES.2003.1238734.

[28] M. Piccardi, "Background subtraction techniques: A review," in *IEEE Int. Conf. Syst. Man Cy.*, Den Hague, The Netherlands, vol. 4, 2004, pp. 3099–3104, doi: 10.1109/ICSMC.2004.1400815.

[29] R. Zetik, S. Crabbe, J. Krajnak, P. Peyerl, J. Sachs, and R. Thomä, "Detection and localization of persons behind obstacles using M-sequence through-the-wall radar," in *Proc. SPIE Sensors, Command, Control, Commun., Intell.*, p. 6201, May 2006, Art. no. 62010I, doi: 10.1117/12.667989.

[30] J. Yang, A. Bouzerdoum, F. H. C. Tivive, and M. G. Amin, "Multiple-measurement vector model and its application to Through-the-Wall radar imaging," in *Proc. IEEE Int. Conf. Acoust., Speech Signal Process. (ICASSP)*, Prague, Czech Republic, May 2011, pp. 2672–2675, doi: 10.1109/ICASSP.2011.5947035.

[31] T. Dogaru and C. Le, "Validation of Xpatch computer models for human body radar signature," Army Res. Lab, Adelphi, MD, USA, Tech. Rep. ARL-TR-4403, Mar. 2008.

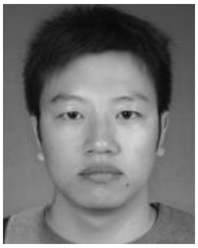

MINCHAO LI was born in Baoji, Shaanxi, China, in 1989. He received the B.S. degree in automation and the M.S. degree in circuits and systems from the Xi'an University of Technology, Xi'an, China, in 2015, where he is currently pursuing the Ph.D. degree in electronic science and technology.

His research interests include signal processing, adaptive filtering algorithms and applications, through-the-wall radar imaging, and machine learning.

XIAOLI XI (Member, IEEE) received the B.S. degree in applied physics from the University of Defense Technology, Changsha, China, in 1990, the M.S. degree in biomedical engineering from Fourth Military Medical University, Xi'an, China, in 1998, and the Ph.D. degree in electrical engineering from Xi'an Jiaotong University, Xi'an, China, in 2004.

She is currently a Professor with the Department of Electronics Engineering, Xi'an University of Technology, Xi'an. Her current research interests include wave propagation, antenna design, and communication signals processing.

XUEHUI ZHANG received the B.S. degree in biomedical engineering from the University of Electronic Science and Technology of China, Chengdu, China, in 2010, and the M.S. and Ph.D. degrees in biomedical engineering from Xi'an Jiaotong University, Xi'an, China, in 2012 and 2015, respectively.

Her current research interests include through-wall radar imaging, signal processing, compressed sensing, and clutter suppression.

GAOHUI LIU received the B.S. degree in electronic engineering and the M.S. degree in signal and information processing from Xidian University, Xi'an, China, in 1991 and 1994, respectively, and the Ph.D. degree in micro-electronics and solid electronics from the Xi'an University of Technology, Xi'an, in 2006.

He is currently an Associate Professor with the Xi'an University of Technology. His current research interests include communication signal processing, passive detection and location, and time synchronization.